JPE 15-1-17

http://dx.doi.org/10.6113/JPE.2015.15.1.177
ISSN(Print): 1598-2092 / ISSN(Online): 2093-4718

Steady-State Integral Proportional Integral Controller for PI Motor Speed Controllers

Choon Lih Hoo*, Sallehuddin Mohamed Haris*, Edwin Chin Yau Chung**, and Nik Abdullah Nik Mohamed***

*Department of Mechanical and Material Engineering, Universiti Kebangsaan Malaysia, Bangi, Malaysia
**School of Eng., Taylor's University Lakeside Campus, Subang Jaya, Malaysia
***German Academic and Career Centre, Universiti Malaysia Pahang, Pekan, Malaysia

Abstract

The output of the controller is said to exceed the input limits of the plant being controlled when a control system operates in a non-linear region. This process is called the windup phenomenon. The windup phenomenon is not preferable in the control system because it leads to performance degradation, such as overshoot and system instability. Many anti-windup strategies involve switching, where the integral component differently operates between the linear and the non-linear states. The range of state for the non-overshoot performance is better illustrated by the boundary integral error plane than the proportional–integral (PI) plane in windup inspection. This study proposes a PI controller with a separate closed-loop integral controller and reference value set with respect to the input command and external torque. The PI controller is compared with existing conventional proportional integral, conditional integration, tracking back calculation, and integral state prediction schemes by using ScicosLab simulations. The controller is also experimentally verified on a direct current motor under no-load and loading conditions. The proposed controller shows a promising potential with its ability to eliminate overshoot with short settling time using the decoupling mode in both conditions.

Key words: Anti-windup, Integral state prediction, PI plane, Speed control, Steady-state integral proportional integral control, Tracking back calculation

I. INTRODUCTION

Several classical and artificial intelligence [1] control schemes have been developed to better track performance, robustness, and stability. These schemes include the H_∞ method [2], neural network [3], fuzzy logic control [4], evolutionary algorithms [5], and hybrid control system [6], which show robustness and better performance in the control of induction and permanent magnet synchronous motors. However, the classical proportional integral derivative (PID) controller has attracted much attention because of its simplicity and ease of implementation. These advantages are reflected by many works that involve optimization and hybrid control system using PID [6].

The inner feedback loop in a variable-speed motor drive is conducted by current control, where the current command must be limited within a prescribed maximum value to prevent any magnetic saturation, motor overheat, and converter protection. The current command generated by the controller exceeds this maximum prescribed input limit when the motor is subjected to sudden input or loading changes. Moreover, the motor exhibits large overshoot, long settling time, and even instability if the PID controller pushes the system into a non-linear region and experiences windup [7]. Based on the reviews in Ref. [7], such performance degradation has been studied since the 1940s. Accordingly, several works have been conducted to investigate the local stability, enforcing stability, and performance properties of the anti-windup compensator.

Several PI-related anti-windup methods (e.g., conditioning technique [8]) have been developed. These methods utilize a

Manuscript received Apr. 5, 2014; accepted Aug. 10, 2014
Recommended for publication by Associate Editor Hyung-Min Ryu.
†Corresponding Author: steven12hcl@gmail.com
Tel: +6012-347-716152, Universiti Kebangsaan Malaysia
*Department of Mechanical and Material Engineering, Universiti Kebangsaan Malaysia, Malaysia
**School of Eng., Taylor's University Lakeside Campus, Malaysia
***German Academic and Career Centre, Universiti Malaysia Pahang, Malaysia

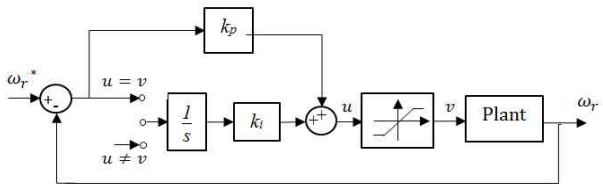

Fig. 1. Block diagram for conditional integral control system.

state feedback integral control with the integrator in the forward path and a dead-zone non-linearity as a feedback. The suitable H and β parameters used in this method promise fast response with little overshoot. The authors in Ref. [9] proposed a variable structure PID (VSPID) to prevent integrator windup. According to Ref. [10], this VSPID allows a system to regain its linearity faster than the anti-windup bumpless transfer technique.

The conditional integration, tracking back calculation, and integral state prediction schemes are the most preferred techniques among the various methods available [11]-[13]. These techniques switch back to the conventional PI control mechanism when the system operates under the linear state. The integral control in the conditional integration system (Fig. 1) stops the error signal accumulation when saturation is detected, thereby separating the integral component from the saturation effect. Accordingly, Ref. [14] also attempted to switch the integral component on and off based on the frequency-domain analysis of the actuator-input command, which ensures a desired tracking performance with minimal oscillation and settling time irrespective of the change in operating conditions.

Meanwhile, Ref. [11] introduced the tracking back calculation scheme (Fig. 2) with a controller feedback signal that consists of the difference between the saturated and the unsaturated control signals. This scheme properly controls the integral state to ensure that the integral state stays within the prescribed control limit. Refs. [11] and [12] introduced the use of the PI plane to inspect the behavior of the control system using the portrayed PI controller output trajectory. The overshoot and the setting time when the PI plane is used are more tightly linked to the attractivity condition. This condition is satisfied if it exhibits asymptotic stability following Lyapunov stability theory. The rise time for any anti-windup scheme is mainly related to the control input limit. Accordingly, Ref. [13] proposed an integral state prediction (ISP) scheme (Fig. 3) based on an analysis using the PI plane. This scheme states that the linear response will have less overshoot and shorter settling time if the integral state right before the system crosses the unsaturation–saturation boundary is close to the steady state integral value. The integral component in this PI control switches between two input channels (i.e., error signal when it is operating in the linear region and the feedback signal during windup). The feedback signal together with the

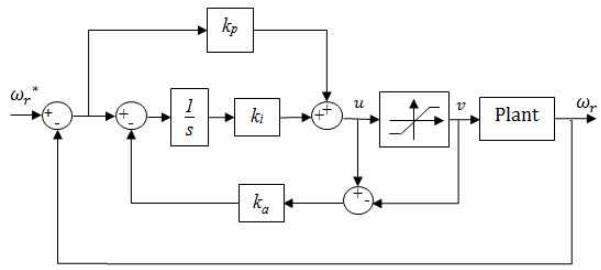

Fig. 2. Block diagram for tracking back calculation scheme.

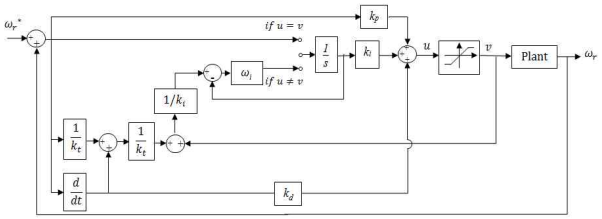

Fig. 3. Block diagram for integral state prediction scheme.

necessary parameters seek an integral steady state. Subsequently, the feedback signal channels the steady state as the input of the integral control component. Therefore, the integral seeks the integral steady state during the saturation state.

This study proposes a steady-state integral PI controller (SIPIC) with a built-in integral controller for variable-speed motor drives that have a different structure from that in the previous work [15]. The proposed SIPIC has a closed-loop integral component that controls and tracks a set reference based on the available system's output and error, and the controller's command signals. Inspired by works on the PI plane, this reference is designed to be the desired steady state integral value even when the system is acted on by an external disturbance/torque. The SIPIC does not involve any switching of the control scheme like those in the other preceding methods. Hence, the SIPIC is free from instability associated with such switching.

The theoretical analysis, simulation, and experimental results for the speed control on a direct current (DC) motor under no load and loading conditions show that the proposed approach with decoupling capability shows a smooth performance curve with no overshoot, zero steady state error, and well-controlled rising time.

II. PI PLANE

The PI plane plots the integral control component ($k_i q$) against the proportional control component ($k_p e$). It also represents the controller's output state at any instant with the allowable maximum and minimum limits for a PI controller's output denoted as B_h and B_l limits, respectively. The following condition [Eq. (1)] is satisfied for the linear operating system:

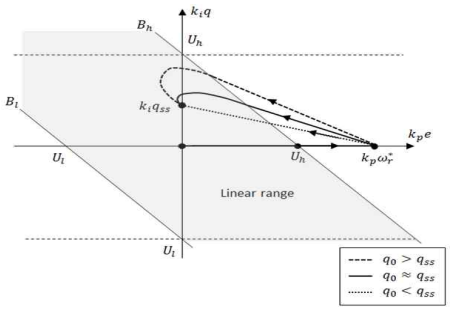

Fig. 4. PI plane.

$$B_l \le k_i q + k_p e \le B_h \tag{1}$$

where k_p and k_i are the proportional and integral tuning parameters, respectively; and e and q are the error and the integral states, respectively. The constraint stated in Eq. (1) is represented as a point in the PI plane within the region bounded between B_h and B_l depicted as a shaded region in Fig. 4. The system operates in a non-linear/saturated state outside this bound.

According to Ref. [13], the amount of overshoot experienced by a system is predicted from the relative value of the integral component when it enters the linear region to its target steady state integral value. A large integral component relative to its steady state value at the time the system regains linearity is found. Accordingly, a large overshoot corresponds to a lower integral component than its target steady state value and slow error response. The path with $q(0)$ and q_{ss} denotes the integral state at the point where the system regains linearity and the target steady state integral value, respectively (Fig. 4). Any trajectory crossing $k_i q$ implies an overshoot as the error changes sign. The shortest response time happens when $q(0) \approx q_{ss}$, which is explained in the discussions that follow.

The following equation is obtained starting with the dynamics error equation for a generic PID controller [Ref. [13] and Eq. (9)]:

$$E(s) = \frac{\frac{k_t k_i}{(1+k_t k_d)}(q_{ss} - q(0))}{s^2 + \left(\frac{\frac{1}{\tau_m} + k_t k_p}{1+k_t k_d}\right)s + \frac{k_t k_i}{1+k_t k_d}} + \frac{e(0)\, s}{s^2 + \left(\frac{\frac{1}{\tau_m} + k_t k_p}{1+k_t k_d}\right)s + \frac{k_t k_i}{1+k_t k_d}} \tag{2}$$

where τ_m, k_t, k_d, and $E(s)$ are the time constant, motor-torque constant, derivative gain, and Laplace form of error signal, respectively. Taking the terms $1/\tau_m + k_t k_p$ as b and $k_t k_i$ as c and considering that $k_d = 0$ for the PI control, the dynamic error equation for the PI controller is expressed in Eq. (3) with its time domain in Eq. (4). Both the k_p and k_i tuning

$$E(s) = \frac{k_t k_i (q_{ss} - q(0)) - \frac{e(0)\left(b - \sqrt{b^2 - 4c}\right)}{2}}{\sqrt{b^2 - 4c}\left(s + \frac{b - \sqrt{b^2 - 4c}}{2}\right)} + \frac{\frac{e(0)\left(\sqrt{b^2 - 4c} + b\right)}{2} - k_t k_i (q_{ss} - q(0))}{\sqrt{b^2 - 4c}\left(s + \frac{b + \sqrt{b^2 - 4c}}{2}\right)} \tag{3}$$

gains appear in the time constant for both terms that describe the system response in Eq. (4). An implication of this is that it is not possible to tune the attribution of each of these terms independently which may be termed as coupled tuning gains. Hence, the rising time of the system cannot be tuned without affecting the settling time, and vice versa. However, the later findings show the possibility of engineering a solution that decouples k_p and k_i.

$$e(t) = \frac{\frac{e(0)\left(b + \sqrt{b^2 - 4c}\right)}{2} - k_t k_i (q_{ss} - q(0))}{\sqrt{b^2 - 4c}} e^{-\left(\frac{b + \sqrt{b^2 - 4c}}{2}\right)t} - \frac{\frac{e(0)\left(b - \sqrt{b^2 - 4c}\right)}{2} - k_t k_i (q_{ss} - q(0))}{\sqrt{b^2 - 4c}} e^{-\left(\frac{b - \sqrt{b^2 - 4c}}{2}\right)t} \tag{4}$$

The time constant for the second term in Eq. (4) is more significant. Hence, the second term dictates the system response from the moment it regains linearity until it arrives at its new steady state. The coefficient of the second term must be positive if no overshoot exists and if the value of the error at the time the system regains linearity $e(0)$ is greater than 0. This result is achieved by equating the coefficient of the second term larger than 0. The condition stated in Eq. (5) must be met, which results from equating the coefficients of the second term to be more than 1. Similarly, the condition for no overshooting stated in Eq. (6) must be met if $e(0) < 0$. Condition (7) must also be met for $e(0) = 0$. Hence, Eqs. (5)–(7) must be met to achieve non-overshoot performance.

$$q(0) < q_{ss} - \frac{e(0)}{k_t k_i}\left(\frac{b - \sqrt{b^2 - 4c}}{2}\right) \tag{5}$$

$$q(0) > q_{ss} - \frac{e(0)}{k_t k_i}\left(\frac{b - \sqrt{b^2 - 4c}}{2}\right) \tag{6}$$

$$q(0) = q_{ss} \tag{7}$$

Based on Eqs. (5)-(7), the boundary integral state, $q(0)$, need not always be close to q_{ss} to avoid overshoot. Conversely, $q(0)$ can have a range of values different from q_{ss} as depicted by the shaded region in Fig. 5 and still not experience overshoot. Therefore, $q(0)$-$e(0)$ plane is a good alternative as a prediction tool for overshoot performance.

III. STEADY STATE INTEGRAL

The operating principle of a PI controller is to have tuning parameters that allow the control system to attain the set reference while performing as desired. The controller's output eventually carries a steady state value that maintains this system output with zero steady state error.

The generic block diagram for a closed-loop system, where the system response [$Y_p(s)$] is detailed in Eq. (8), is presented in Fig. 6. $C(s)$ and $G(s)$ denote the transfer function of the controller and the plant, respectively. $U(s)$ and $T(s)$ are the input reference and the torque that affects the plant, respectively.

$$Y_p(s) = \frac{U(s)C(s)G(s) - T(s)G(s)}{1 + C(s)G(s)} \tag{8}$$

The controller's output signal is obtained by taking its output as the output of a closed-loop system (Fig. 7). Similarly, the output of the controller is described in detail as follows:

$$Y(s) = \frac{U(s)C(s) + T(s)G(s)C(s)}{1 + C(s)G(s)} \tag{9}$$

The DC gain of the PI controller in the closed-loop configuration for an nth order plant with a generic transfer function described in Eq. (10) is depicted in Fig. 7. Its steady state is described in Eq. (11). a_i and b_i are the coefficients in Eq. (10) along with m, $n \in \mathbb{N}^+$, and $m \leqslant n$.

The steady state output of the PI controller is affected by the input reference, plant parameters, and the torque that affects the system. The torque term is not present in the steady state expression if no external torque acts on the plant.

$$G(s) = \frac{a_m s^m + a_{m-1}s^{m-1} + a_{m-2}s^{m-2} + \cdots + a_1 s^1 + a_0}{b_n s^n + b_{n-1}s^{n-1} + b_{n-2}s^{n-2} + \cdots + b_1 s^1 + b_0} \tag{10}$$

$$\lim_{s \to 0} sY(s) = \frac{U(s)b_0}{a_0} + T(s) \tag{11}$$

This finding is used to verify the validity of the analysis in the subsequent section.

IV. LINEAR RANGE OF PI CONTROL

A variable-speed motor drive is usually designed with an inner current controller having a much faster dynamics than its outer speed controller. Accordingly, the dynamics of a variable-speed motor drive considering the loading effect is given by Eq. (12), where ω_r, T_l, and v denote the rotational motor speed, external torque/disturbance, and plant input, respectively. The output of the PI controller, u, which comprises proportional gain, k_p, integral gain, k_i, input error, e, and integral state, q, parameters, is indicated in Eq. (13). The error of the closed-loop system for a variable-speed motor drive is obtained from the difference between the current speed of the motor and the set reference [Eq. (14)] with ω_r^* as the set reference or command.

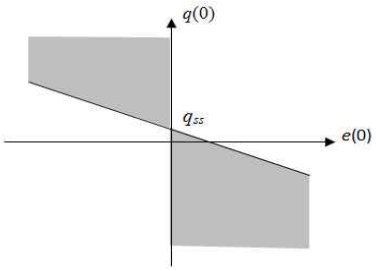

Fig. 5. Graph of $q(0)$ against $e(0)$ and regions where a PI control system is free from overshoot as it recovers from windup.

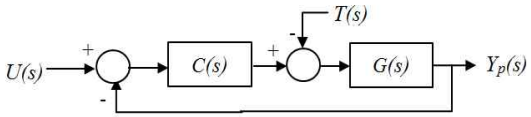

Fig. 6. Block diagram of a closed loop system.

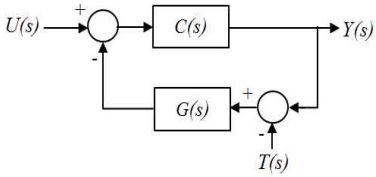

Fig. 7. Block diagram of a closed loop system with the controller as output.

$$\frac{d\omega_r}{dt} = -\frac{1}{\tau_m}\omega_r + k_t v - T_l \tag{12}$$

$$u = k_p e + k_i q \tag{13}$$

$$e = \omega_r^* - \omega_r \tag{14}$$

At steady state, Eq. (12) is rewritten as Eq. (15) because ω_r remains constant, the error is eliminated, and $v = k_i q_{ss}$. The equation is further rearranged to show that $k_i q_{ss}$, which is the steady state integral component of the PI controller, has an expression described in Eq. (16). Correspondingly, Eq. (16) has a similar structure to Eq. (11). T_l is not a signal that is readily available as input to a controller in practice. However, T_l from Eq. (12) is derived from available signals. Substituting Eqs. (12) and (14) into Eq. (15), the steady state integral is expressed in terms of the available signals described in Eq. (17).

$$0 = -\frac{1}{\tau_m}\omega_r^* + k_t k_i q_{ss} - T_l \tag{15}$$

$$k_i q_{ss} = \frac{T_l}{k_t} + \frac{\omega_r^*}{k_t \tau_m} \tag{16}$$

$$k_i q_{ss} = v - \frac{\dot{\omega}_r}{k_t} + \frac{e}{k_t \tau_m} \tag{17}$$

V. PROPOSED SIPIC

Continuing with our line of analysis, the output of the PI controller, u, for a PI-controlled variable-speed motor drive is identical to the input to the motor drive, v, when it is

operating in the linear region. The dynamics of the PI-controlled variable-speed motor drive is described in Eq. (12) in a closed-loop configuration. The rotational motor speed is specified in terms of the closed-loop error shown in Eq. (18) substituted into Eq. (12). The error of the closed-loop PI-controlled variable-speed motor drive system is expressed in Eq. (19).

$$\omega_r = \omega_r^* - e \tag{18}$$

$$-\dot{e} = \left(\frac{1}{\tau_m} + k_t k_p\right)e + k_t k_i q - \frac{1}{\tau_m}\omega_r^* - T_l \tag{19}$$

The last two terms in Eq. (19) at steady state denote the steady state integral in Eq. (16). The Laplace domain form of the error dynamics is presented in Eq. (20).

$$E(s) = \frac{e(0) + k_t k_i\left(\frac{q_{ss}}{s} - Q(s)\right)}{\left(s + \frac{1}{\tau_m} + k_t k_p\right)} \tag{20}$$

For a good system design, there ought to be no steady state error in the system, $e(\infty) = 0$. This essentially translates to the design for the integral component in (20) such that the condition stated in equation (21) is met. This can be further translated into the condition that the expression in the bracket of Eq. (21) reduces into a function of s that does not have any pole at the origin. With this, a possible generic format for this function may be that described in Eq. (22) where A and B are constant and n is a non-negative integer.

The preceding discussion indicates that the integral component and structure of the PI controller depend on how the function on the right-hand side of Eq. (22) is defined. Moreover, the pole(s) of this integral component will eventually be the pole(s) for the error response in Eq. (20). This finding is important because each pole contributes and determines the system performance. One of the poles of the error in Eq. (20) already consists of the k_p tuning parameter. Hence, designing the right-hand side of Eq. (22) with only the k_i tuning parameter and without the k_p tuning parameter would decouple k_p and k_i. Consequently, decoupling solves the difficulty of choosing controller gains that allow the coexistence of non-overshoot and short settling time. The function that ultimately defines $Q(s)$ needs to be a function that can be implemented in practice.

$$\lim_{s\to 0} k_t k_i s\left(\frac{q_{ss}}{s} - Q(s)\right) = 0 \tag{21}$$

$$\frac{q_{ss}}{s} - Q(s) = \mathrm{A}s^n f(s) + \mathrm{B} \tag{22}$$

One possible combination of A, B, and n is described in Eq. (23), which introduces an integral component of the PI controller in Eq. (24) (Fig. 8). The $k_i q_{ss}$ in Fig. 8 is implemented using known terms, speed derivative, error signal, and plant input expressed in Eq. (17) by channeling the necessary feedback signals. This setup leads to the PI controller depicted in Fig. 9.

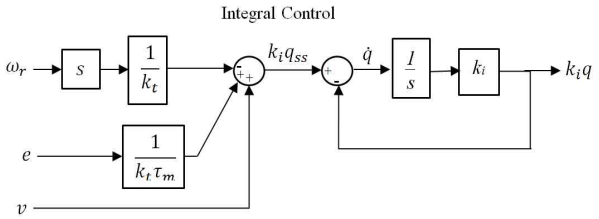

Fig. 8. Proposed integral component of SIPIC.

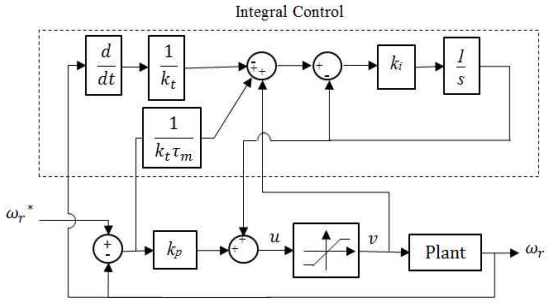

Fig. 9. Block diagram for the proposed SIPIC.

$$\frac{q_{ss}}{s} - Q(s) = \frac{1}{k_i}\left(sQ(s) - q(0)\right) \tag{23}$$

$$k_i\left(q_{ss} - q\right) = \dot{q} \tag{24}$$

A. Characteristic Analysis

Instead of a straight integration of the error to derive the integral component of the PI controller from Eq. (23), the integral component of the SIPIC is expressed in Eq. (25). The error equation for the SIPIC is shown in Eq. (26) through the substitution of Eq. (25) into Eq. (20). The SIPIC is easily proven to have a zero steady state error when s approaches zero. Compared with the existing anti-windup schemes, the SIPIC does not need to switch its integral control component to another scheme during saturation and also does not suffer from any associated adverse effect.

$$Q(s) = \frac{k_i q_{ss} + q(0)s}{s(s + k_i)} \tag{25}$$

$$\begin{aligned} E(s) &= \frac{e(0)}{s + 1/\tau_m + k_t k_p} \\ &\quad + \frac{k_t k_i\left(q_{ss} - q(0)\right)}{\left(s + k_i\right)\left(s + 1/\tau_m + k_t k_p\right)} \\ &= \frac{e(0)\left(s + k_i\right) + k_t k_i\left(q_{ss} - q(0)\right)}{\left(s + k_i\right)\left(s + 1/\tau_m + k_t k_p\right)} \end{aligned} \tag{26}$$

The error response of the SIPIC, which is translated into the time domain, is described in Eq. (27). The first term of this expression determines the response of the SIPIC to a perturbation, whereas the second term gives its error convergence pattern. The k_p and k_i tuning parameters are separated in the error response expression. Hence, these parameters can be tuned to have no overshoot and still maintain a zero steady state error. In contrast, it is common for a conventional PI controller where a short rise time will induce overshoot.

TABLE I
PARAMETERS OF DC MOTOR

Moment of inertia (J)	2.14×10^{-5} kg m^2
Viscous damping coefficient (B)	2.11×10^{-4} kg m^2/s
Time constant (τ_m)	0.02 s
Torque constant (k_T)	0.09 N m/A
Inductance (L)	0.005 H
Resistance (R)	7.8 Ω

$$e(t) = \left\{ e(0) - \left[\frac{k_t k_i (q_{ss} - q(0))}{1/\tau_m + k_t k_p - k_i} \right] \right\} e^{-(1/\tau_m + k_t k_p)t} + \left[\frac{k_t k_i (q_{ss} - q(0))}{1/\tau_m + k_t k_p - k_i} \right] e^{-k_i t} \quad (27)$$

B. Lyapunov Stability

The Lyapunov function candidate described in Eq. (28) is considered to examine the SIPIC stability. For simplicity and since the integral controller in the SIPIC has embedded in it the theoretical steady state value, the time derivative of the Lyapunov function candidate can be written as shown in Eq. (29). Substituting the derivative of e with the expression in Eq. (19) gives the expression in Eq. (30). Moreover, substituting $k_i q_{ss}$ with its equivalent from Eq. (16) gives Eq. (31). $\dot{V}(e) < 0$ indicates that the system is asymptotically stable.

$$V(e) = \frac{1}{2k_t} e^2 \quad (28)$$

$$\dot{V}(e) = \frac{1}{k_t} e\dot{e} \quad (29)$$

$$\dot{V}(e) = -\frac{e^2}{k_t \tau_m} - k_p e^2 - e\left(k_i q_{ss} - \frac{\omega_r^*}{k_t \tau_m} - \frac{T_l}{k_t} \right) \quad (30)$$

$$\dot{V}(e) = -\left(\frac{e^2}{k_t \tau_m} + k_p e^2 \right) \quad (31)$$

C. q(0)–e(0) Graph for SIPIC

The natural frequency (ω_n) and the damping ratio (ζ) of the SIPIC are described in Eqs. (32) and (33), respectively, as extracted from the denominator of Eq. (26). The damping ratio (ζ) in Eq. (33) must be less than 1 for this system to exhibit overshoot. Equating Eq. (33) to be less than 1 and rearranging eventually translate into the condition detailed in Eq. (34). This condition is only satisfied if the expression in the bracket is a complex number. However, this condition is never satisfied because these gains and system parameters are real numbers. This result indicates that the SIPIC will not experience an overshoot irrespective of the values of these controller gains and system parameters. As discussed in Section IIA, the SIPIC is also free from the constraints on $e(0)$ and $q(0)$ to avoids overshoots unlike a generic PID controller.

Fig. 10. Experimental setup for DC motor speed control.

$$\omega_n = \sqrt{k_i (1/\tau_m + k_t k_p)} \quad (32)$$

$$\zeta = \frac{k_i + 1/\tau_m + k_t k_p}{2\sqrt{k_i (1/\tau_m + k_t k_p)}} \quad (33)$$

$$[k_i - (1/\tau_m + k_t k_p)]^2 < 0 \quad (34)$$

VI. SIMULATION AND EXPERIMENTAL RESULTS

The performance of the SIPIC for controlling the speed of a direct current (DC) motor is compared with that of the conventional PI, conditional integration, tracking back calculation, and integral state prediction schemes to validate the SIPIC characteristic. These comparison analyses were performed using ScicosLab simulations and hardware testing for no-load and loading conditions. A metal plate is attached to the motor shaft to introduce a 8.63×10^{-5} kg m^2 moment of inertia into the motor serving as a constant loading condition. Table I presents the DC motor specifications used in these simulations and testing. The experimental test rig with a PC base DAQ and a two-time voltage amplifier is shown in Fig. 10. The speed command for these simulations and testing is set to 100 rad/s from the start and decreased to −100 rad/s at time t = 1s with a voltage limiter of 15 V. Different sets of PI gains are used for the no-load and loading conditions to better illustrate the significant improvement in both conditions when the SIPIC is used.

A. No-Load Scenario

The simulated motor speed of the proposed SIPIC controller, conventional PI, conditional integration, tracking back calculation, and integral state prediction schemes under the no-load condition for two different sets of tuning gains is presented in Fig. 11 and 12. All these methods ultimately reach the desired speed. However, they differ in their integral component [Fig. 11(b) and 12(b)]. On the one hand, the conditional integration scheme switches off its integral component during saturation. On the other hand, the integral of the tracking back calculation, ISP, and the proposed SIPIC determines the steady state value with respect to the input command and external torque condition regardless if the system is operating in the linear or the non-linear region or not. The proposed SIPIC has the shortest settling time.

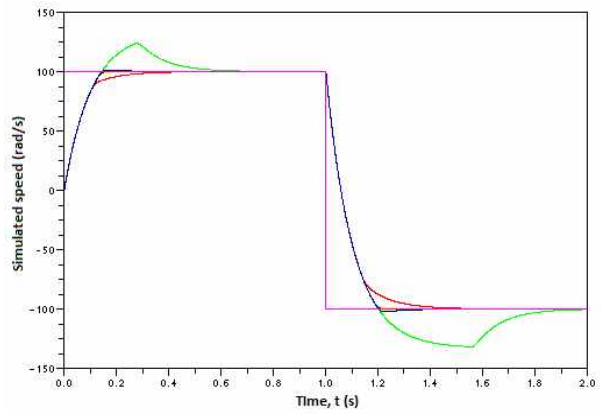

(a)

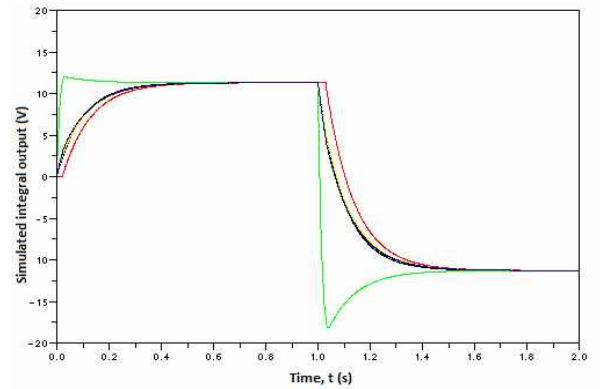

(b)

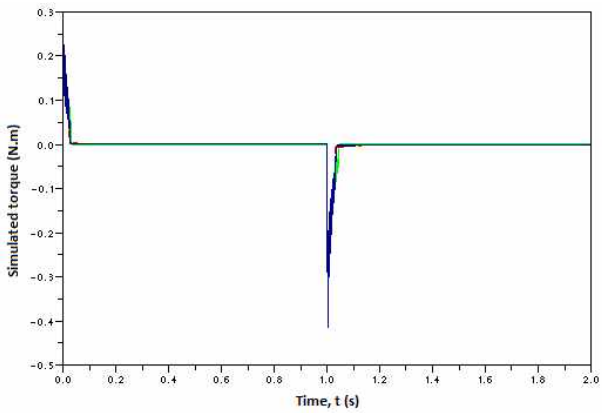

(c)

Fig. 11. Simulation comparison of the anti-windup schemes for the DC motor control with a changing step input at the no-load condition for $k_p = 1$ and $k_i = 10$ (purple: reference, green: PI, red: conditional integration, yellow: ISP, blue: tracking back calculation, and black: SIPIC). (a) Speed, (b) integral output, and (c) torque.

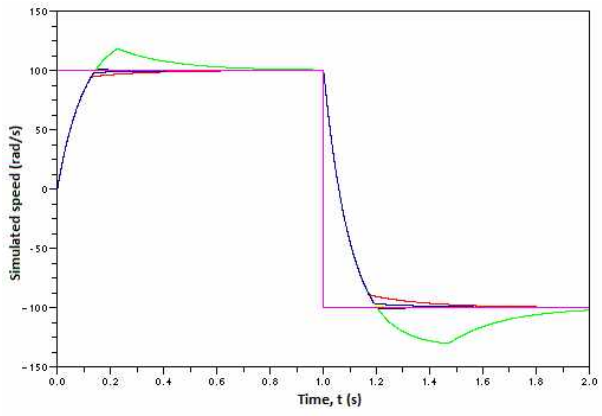

(a)

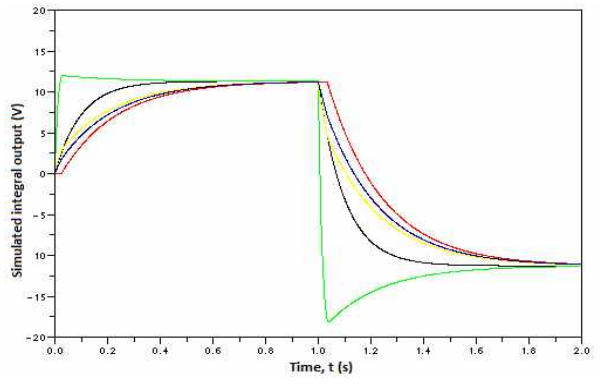

(b)

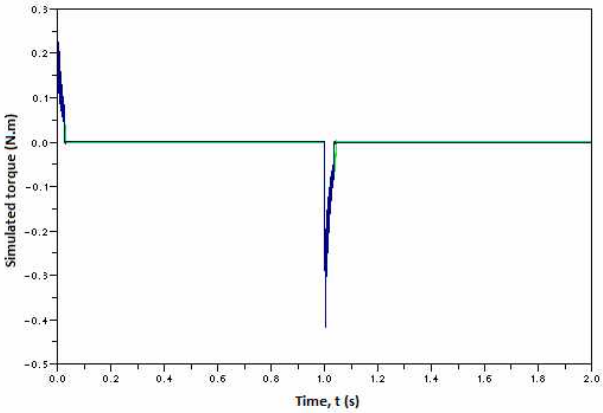

(c)

Fig. 12. Simulation comparison of the anti-windup schemes for the DC motor control with a changing step input at the no-load condition for $k_p = 2$ and $k_i = 10$ (purple: reference, green: PI, red: conditional integration, yellow: ISP, blue: tracking back calculation, and black: SIPIC). (a) Speed, (b) integral output, and (c) torque.

The experimental results for the motor speed and its integral component for different tuning parameter sets are shown in Figs. 13 and 14, respectively. These two parameters perform similarly in the simulation. The existing anti-windup schemes still behave differently because of the difference in their $q(0)$ and $e(0)$ values even though they switch to a conventional PI controller in the unsaturated region. The conditional integration scheme does not suffer from any overshoot. However, it takes a longer path than the SIPIC and experiences a slower error response. The settling time of the

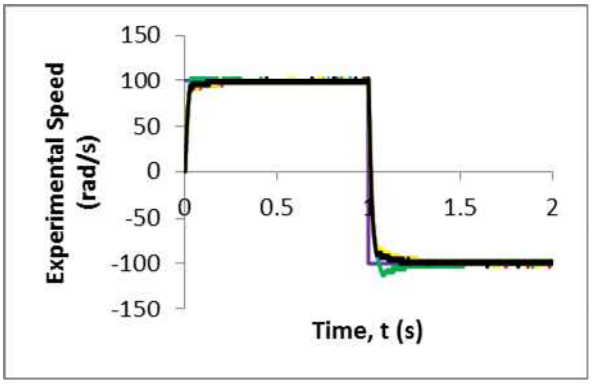

(a)

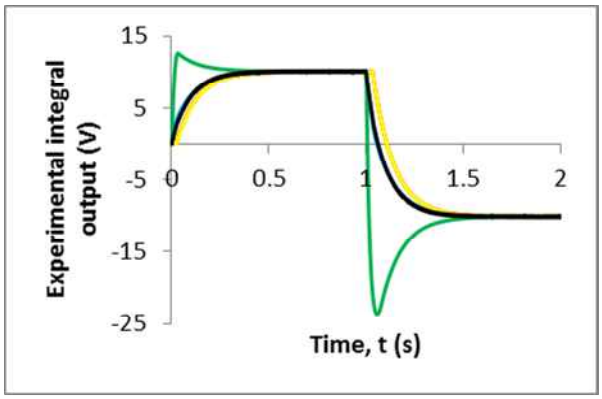

(b)

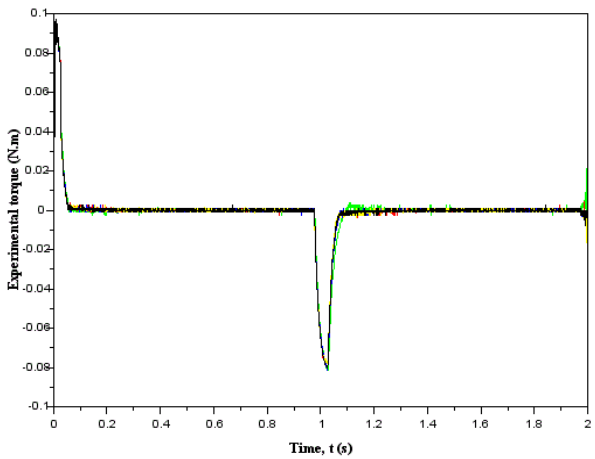

(c)

Fig. 13. Experimental comparison of the anti-windup schemes for the DC motor control with a changing step input at the no-load condition for $k_p = 1$ and $k_i = 10$ (purple: reference, green: PI, red: conditional integration, yellow: ISP, blue: tracking back calculation, and black: SIPIC). (a) Speed, (b) integral output, and (c) torque.

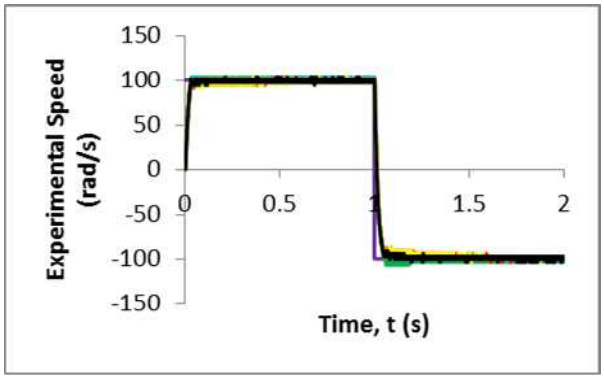

(a)

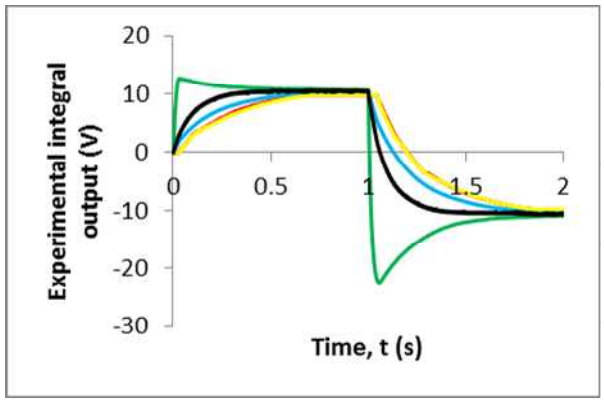

(b)

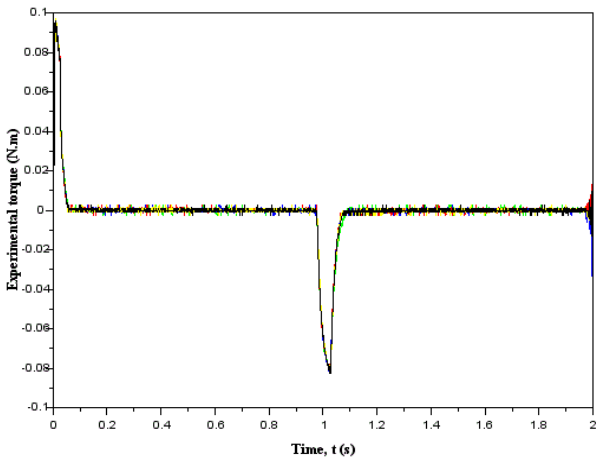

(c)

Fig. 14. Experimental comparison of the anti-windup schemes for the DC motor control with a changing step input at the no-load condition for $k_p = 2$, $k_i = 10$ (purple: reference, green: PI, red: conditional integration, yellow: ISP, blue: tracking back calculation, and black: SIPIC). (a) Speed, (b) integral output, and (c) torque.

conditional integration, tracking back calculation, and ISP reduces when the k_p value is increased. By comparison, the proposed SIPIC experiences little to no overshoot and has the shortest settling time among the schemes. This finding is supported by the torque response curve. Based on Figs. 11(c), 12(c), 13(c), and 14(c), the SIPIC has better control on the torque change.

B. Loading Scenario

The simulated motor performance of the five schemes

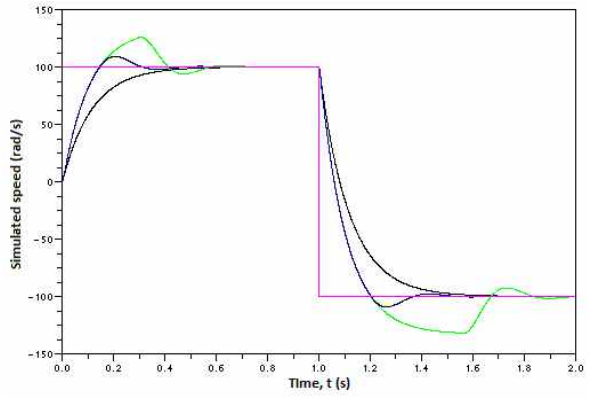

(a)

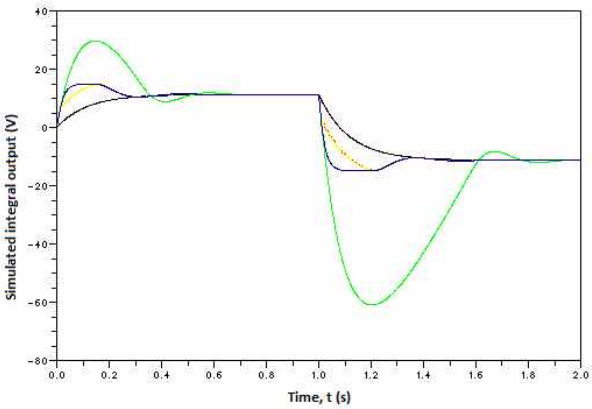

(b)

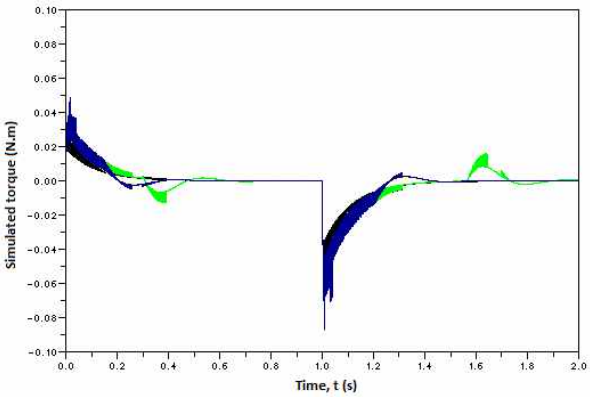

(c)

Fig. 15. Simulation comparison of the anti-windup schemes for the DC motor control with a changing step input under the loading condition for $k_p = 0.1$ and $k_i = 5$ (purple: reference, green: PI, red: conditional integration, yellow: ISP, blue: tracking back calculation, and black: SIPIC). (a) Speed, (b) integral output, and (c) torque.

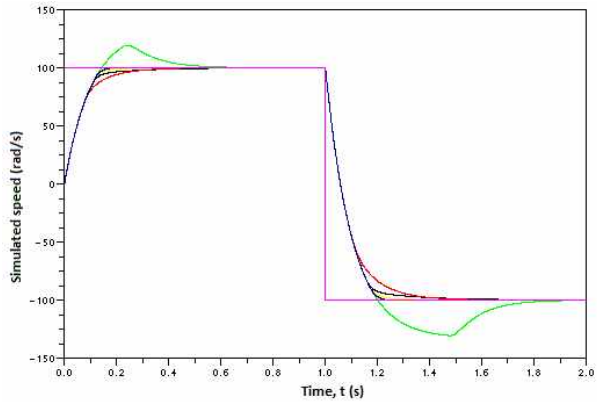

(a)

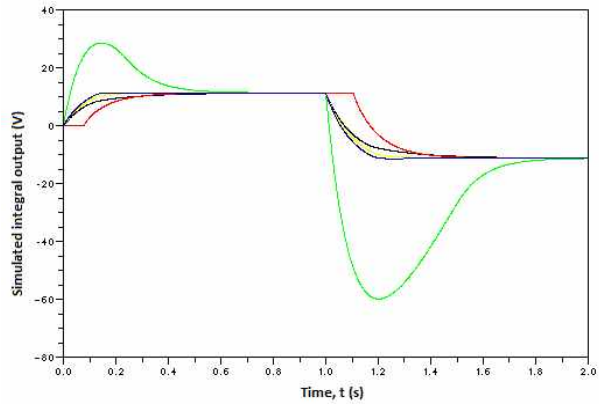

(b)

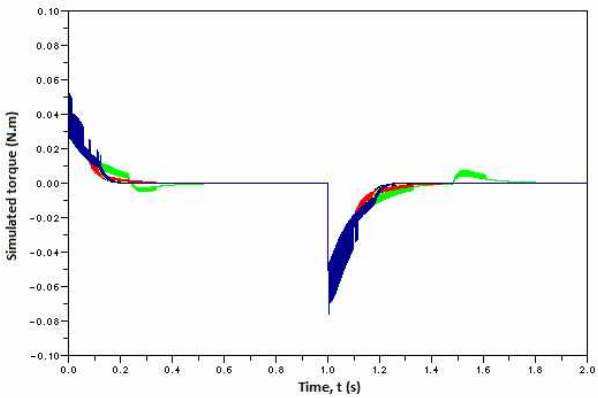

(c)

Fig. 16. Simulation comparison of the anti-windup schemes for the DC motor control with a changing step input under the loading condition for $k_p = 0.5$ and $k_i = 5$ (purple: reference, green: PI, red: conditional integration, yellow: ISP, blue: tracking back calculation, band lack: SIPIC). (a) Speed, (b) integral output, and (c) torque.

under the loading condition at the k_p and k_i values is presented in Figs. 15–17. All schemes have longer rise and settling times compared with that in the no-load scenario. Furthermore, the existing schemes experience overshoot under a low k_p value. The SIPIC produces the shortest settling time and with no overshoot. The short settling time without overshoot at high k_p value is actually attributed to the decoupling mode, which provides the possibility of having the desired short settling time while maintaining non-overshoot performance. The same observation, which

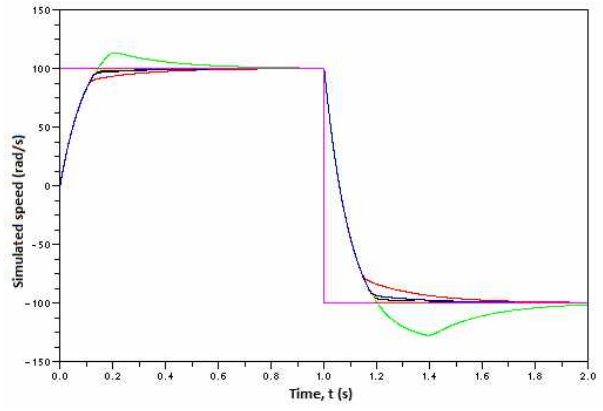

(a)

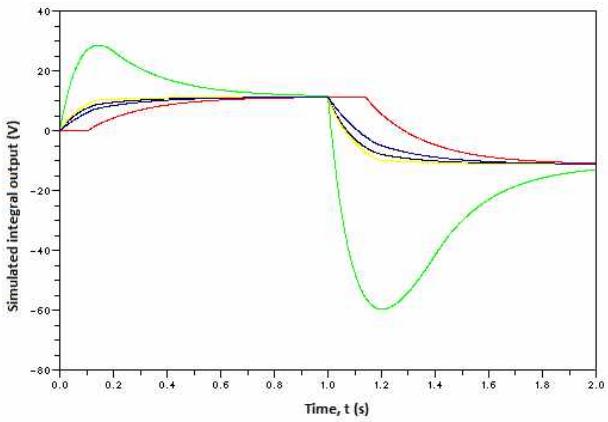

(b)

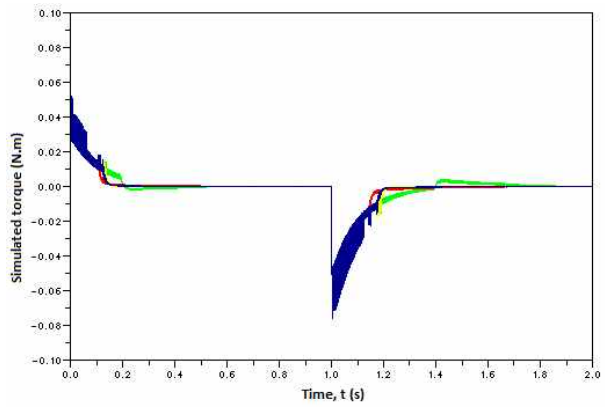

(c)

Fig. 17. Simulation comparison of the anti-windup schemes for the DC motor control with a changing step input under the loading condition for $k_p = 1$ and $k_i = 5$ (purple: reference, green: PI, red: conditional integration, yellow: ISP, blue: tracking back calculation, and black: SIPIC). (a) Speed, (b) integral output, and (c) torque.

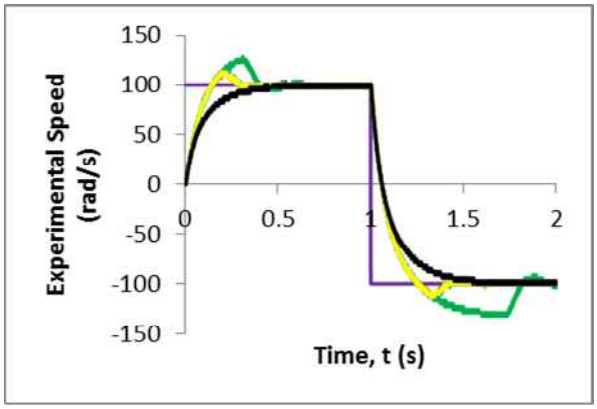

(a)

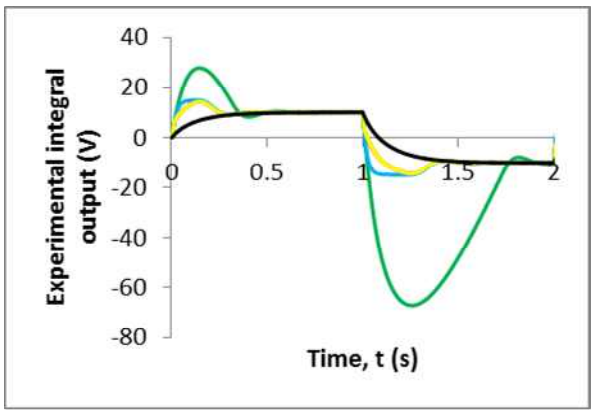

(b)

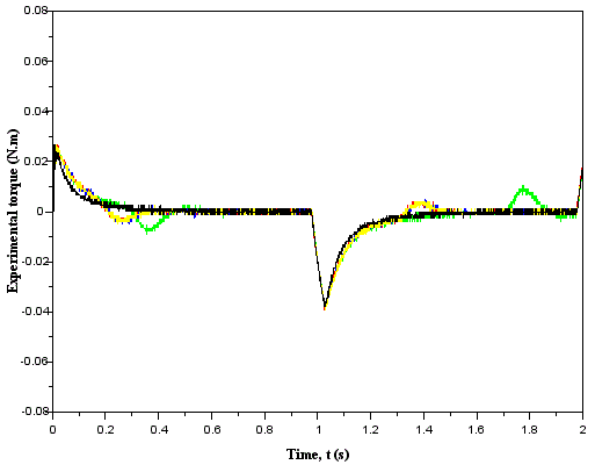

(c)

Fig. 18. Experimental comparison of the anti-windup schemes for the DC motor control with a changing step input under the loading condition for $k_p = 0.1$ and $k_i = 5$ (purple: reference, green: PI, red: conditional integration, yellow: ISP, blue: tracking back calculation, and black: SIPIC). (a) Speed, (b) integral output, and (c) torque.

corresponds to their integral components reaching the steady state slower than the SIPIC, is shown in Figs. 18–20. The ISP slants in reaching the desired state even though it has a rapid rise of integration.

The PI control output in both scenarios always suffers from saturation and exhibits overshoot because of the windup and coupling behavior. The integral output graphs show that each scheme employs a different integral state value. The

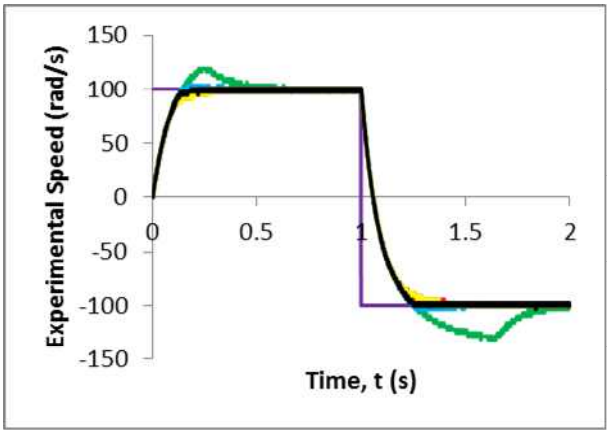

(a)

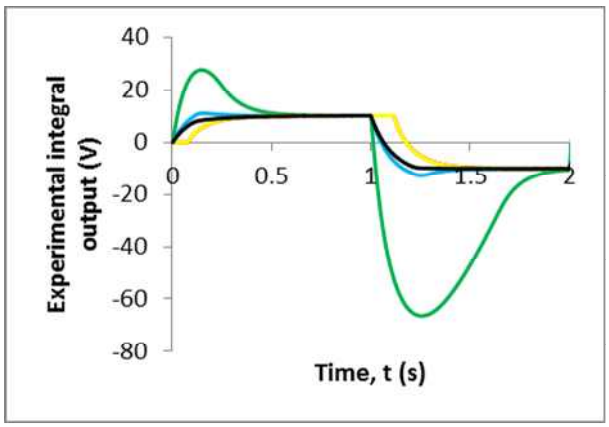

(b)

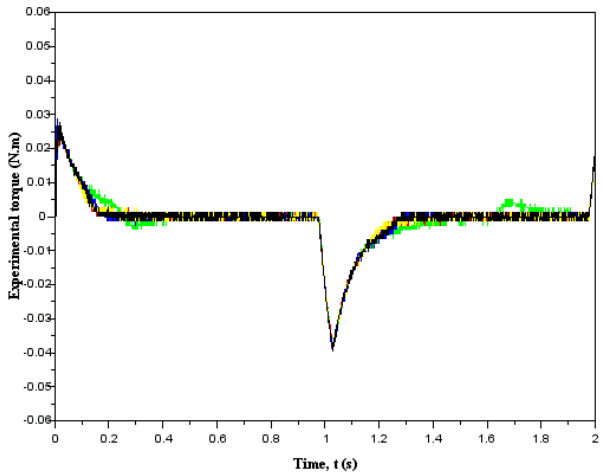

(c)

Fig. 19. Experimental comparison of the anti-windup schemes for the DC motor control with a changing step input under the loading condition for $k_p = 0.5$ and $k_i = 5$ (purple: reference, green: PI, red: conditional integration, yellow: ISP, blue: tracking back calculation, and black: SIPIC). (a) Speed, (b) integral output, and (c) torque.

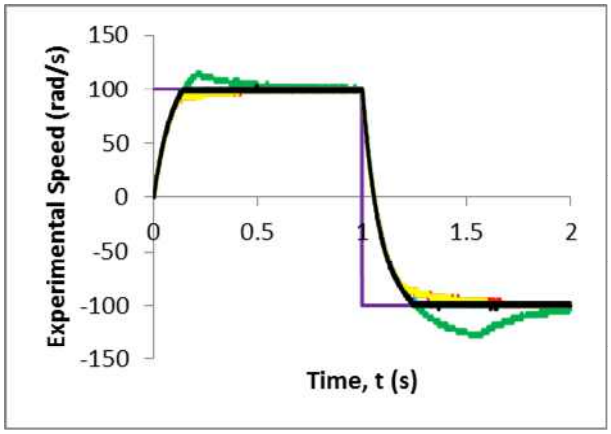

(a)

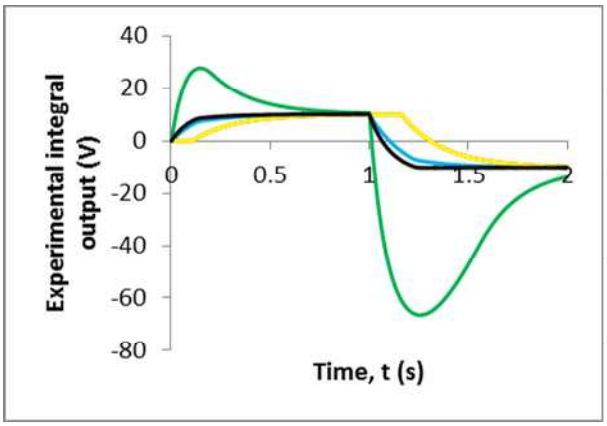

(b)

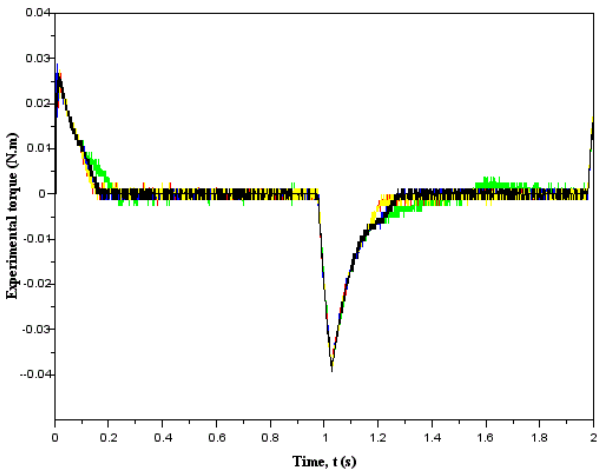

(c)

Fig. 20. Experimental comparison of the anti-windup schemes for the DC motor control with a changing step input under the loading condition for $k_p = 1$ and $k_i = 5$ (purple: reference, green: PI, red: conditional integration, yellow: ISP, blue: tracking back calculation, and black: SIPIC). (a) Speed, (b) integral output, and (c) torque.

tracking back calculation sets a higher value than the actual steady state value. The conditioning scheme remains at zero integral, whereas the ISP and the SIPIC maintain a constant steady state value. The inclined boundary lines promise faster

entry to the linear region for boundary integral states lower than the steady-state value. The conditional integration experiences a short saturation duration, which is followed by the SIPIC, ISP, and the tracking back calculation scheme. The conventional PI scheme exhibits the longest duration. Moreover, uncertainty in the value of the integral state occurs when the integral component is switched off. Hence, the switching of the integral stage method does not guarantee the fastest re-entry into the linear range in every case. The conditional integration also suffers from overshoot if the value held is higher than the steady state during the switching. With regard to the torque, the SIPIC has a faster response to torque change and less fluctuation before regaining stability.

VII. Conclusions

The proposed SIPIC is another new integral anti-windup scheme with a separately sourced integral closed-loop controller that carries the desired steady state value based on the respective input command throughout the unloading or loading operating conditions. The integral signal transfers into the system from the closed loop and engages with the PI controller, which is directed with the error signal and makes the PI controller. As comparison with the existing methods, the proposed SIPIC shows promising results. The integral control of the SIPIC reaches and stays at the steady state even during saturation. In addition, the SIPIC takes a shorter path when moving toward the steady state without overshooting. As a summary, the SIPIC shows better performance in both conditions than the existing methods. Based on the theoretical analysis and experimental work, the SIPIC is believed to work for any first-order application.

Acknowledgement

Thanks to Mr. Tan Chin Luh of Trity Technologies for sharing useful information and assisting the simulation and hardware testing.

References

[1] R. A. Gupta, R. Kumar, and A. K. Bansal, "Artificial intelligence applications in Permanent Magnet Brushless DC motor drives," *Artificial Intelligence Review,* Vol. 33, No. 3, pp. 175-186, Mar. 2010.

[2] C. L. Lin and H. Y. Jan, "Application of evolution strategy in mixed H_∞/H_2 control for a linear brushless DC motor," in *2003 IEEE/ASME International Conference on Advanced Intelligent Mechatronics, 2003. AIM 2003 Proceedings*, pp. 1-6, 2003.

[3] B. K. Bose, "Neural network applications in power electronics and motor drives-an introduction and perspective," *IEEE Trans. Ind. Electron.*, Vol.54, No. 1, pp. 14-33, Feb. 2007.

[4] L. F. Baptista, J. M. Sousa, and J. M. G. Sá da Costa, "Fuzzy predictive algorithms applied to real-time force control," *Control Engineering Practice,* Vol. 9, No. 4, pp. 411-423, Apr. 2001.

[5] P. J. Fleming and R. C. Purshouse, "Evolutionary algorithms in control systems engineering: A survey," *Control Engineering Practice,* Vol. 10, No. 11, pp. 1223-1241, Nov. 2002.

[6] S. M. Gadoue, D. Giaouris, and J. W. Finch, "Artificial intelligence-based speed control of DTC induction motor drives – A comparative study," *Electric Power Systems Research,* Vol. 79, No. 1, pp. 210-219, Jan. 2009.

[7] S. Tarbouriech and M. Turner, "Anti-windup design: An overview of some recent advances and open problems," *IET Control Theory Appl.*, Vol. 3, No. 1, pp. 1-19, Mar. 2009.

[8] N. J. Krikelis, "State feedback integral control with intelligent integrator," *Int. J. Control*, Vol. 32, No. 3, pp. 465-473, Mar. 1980.

[9] A. S. Hodel and C. E. Hall, "Variable-structure PID control to prevent integrator windup," *IEEE Trans. Ind. Electron.*, Vol. 48, No. 2, pp. 442-451, Apr. 2001.

[10] R. Mantz and H. De Battista, "Authors' replay to comments on "Variable-Structure PID Control to Prevent Integrator Windup"," *IEEE Trans. Ind. Electron.,* Vol. 51, No. 3, pp. 736-738, Jun. 2004.

[11] J. K. Seok, "Frequency-spectrum-based antiwindup compensator for PI controlled systems," *IEEE Trans. Ind. Electron.*, Vol. 53, No. 6, pp. 1781-1790, Dec. 2006.

[12] H.-B. Shin, "New antiwindup PI controller for variable-speed motor drives," *IEEE Trans. Ind. Electron.*, Vol. 45, No. 3, pp. 445-450, Jun. 1998.

[13] X.-L. Li, J.-G. Park, and H.-B. Shin, "Comparison and evaluation of anti-windup PI controllers," *Journal of Power Electronics,* Vol. 11, No. 1, pp. 45-50, Jan. 2011.

[14] H.-B. Shin and J.-G. Park, "Anti-Windup PID Controller With Integral State Predictor for Variable-Speed Motor Drives," *IEEE Trans. Ind. Electron.,* Vol. 59, No. 3, pp. 1509-1516, Mar. 2012.

[15] C. L. Hoo, C. Y. Edwin Chung, S. M. Haris, and N. A. N. Mohamed, "New proportional integral controller for Nth order transfer function model," in *Third Int. Conf. on Control, Automation and Systems Engineering (CASE)*, pp. 28-29, 2013.

Choon Lih Hoo graduated from the Universiti Kebangsaan Malaysia, Bangi, Malaysia in 2009 with a B.Eng. in Mechanical Engineering. He is a Ph.D. candidate in the same university. He is currently a lecturer at Taylor's University Lakeside Campus, Malaysia. His research interests include control system, FPGA, and artificial intelligence.

Sallehuddin Mohamed Haris obtained his B.Eng. degree in Manufacturing Systems Engineering in 1993, his MSc degree in Mechatronics in 1996, and his Ph.D. in Electronics and Electrical Engineering in 2006 in the United Kingdom. His current research interests include the development of control algorithms for hybrid and switched dynamic systems, autonomous robot control based on monocular vision, and mechatronic systems for automotive applications.

Edwin Chin Yau Chung holds a Ph.D. in Electrical and Computer Systems Engineering from Monash University (Australia). He also has a B.Eng. with First Class Honors in the same field and a.Sc. in Computer Science. He has published many papers on asynchronous circuit design and holds a patent in the field of telecommunication. Since 1995, he has worked with international companies such as Intel, Motorola, and NEC. He is currently the director of Taylor's Technology Innovation Centre.

Nik Abdullah Nik Mohamed obtained his Ing. Grad. (B.E) at the University of Applied Science in Munich, Germany, in 1979. He obtained the Diplom-Ingenieur (M.S) in 1983 followed by his Dr-Ing. (Ph.D) in 1991 in Germany. He is a professor, and his fields of specialization include continuum mechanics and constitutive equations, smart materials and structures, and reliability and maintainability engineering. He is affiliated with the German Academic & Career Centre of Universiti Pahang Malaysia.